Aust. J. Phys., 1987, **40**, 713–24

Old Supernova Remnants: Structure and Source of Radio Emission*

A. P. Glushak, A. V. Kovalenko, S. M. Kutuzov, A. V. Pynzar' and V. A. Udal'tsov

Lebedev Physical Institute, USSR Academy of Sciences,
117924 Leninsky Pr., 53 Moscow, USSR.

Abstract

Contour maps at 102·5 MHz for 12 galactic SNRs of large angular size in the northern sky are presented. The observations were made with an angular resolution of $48' \times 24' \sec(55° - \delta)$ using the BSA telescope of the Lebedev Physical Institute. All sources were mapped in total intensity. Our results indicate that the contribution to the radiation of observed SNRs from swept up cosmic ray electrons is small. The characteristics of the observed sources are discussed.

1. Introduction

Supernova remnants (SNRs) with low surface brightness and linear sizes more than 30 pc are referred to as old SNRs (with an age more than 10^4 yr). According to the model by Van der Laan (1962) the main source of radio emission from such remnants is relativistic electrons in the interstellar medium swept up by the shock wave of the SNR (Shklovskii 1960; Gull 1973). For young SNRs, the relativistic electrons are injected during the burst, accelerated on the shock wave front or injected by the supernova relic (neutron star–pulsar), as in the Crab Nebula (Weiler and Panagia 1978). Thus in old SNRs, the relativistic electrons responsible for radio emission are derived from the interstellar medium, whereas in young remnants they arise from the supernova itself. It follows then that the ratio of relativistic electrons of a given energy connected with supernovae and the interstellar medium must change with time. This can be shown by estimates of the ratio of the total energy of relativistic electrons of old SNRs and the energy of interstellar cosmic ray electrons in the SNR volume, which have been swept up by the supernova shock. For this purpose and for deriving structure, scale size, spectrum and flux density of old SNRs in the northern hemisphere at metre wavelengths, a number of old SNRs have been mapped at a frequency of 102·5 MHz using the total power method.

2. Observations

Observations were carried out with the BSA radio telescope of the Lebedev Physical Institute (Vitkevich *et al.* 1976) in Pushchino. The BSA is a phased two-dimensional array consisting of full-wave dipoles. The BSA has an effective aperture of 4×10^4 m^2

* Paper presented at the Joint USSR–Australia Shklovskii Memorial Symposium on Supernova Remnants and Pulsars, held at Pushchino, USSR, 8–11 June 1986.

0004-9506/87/060713$02.00

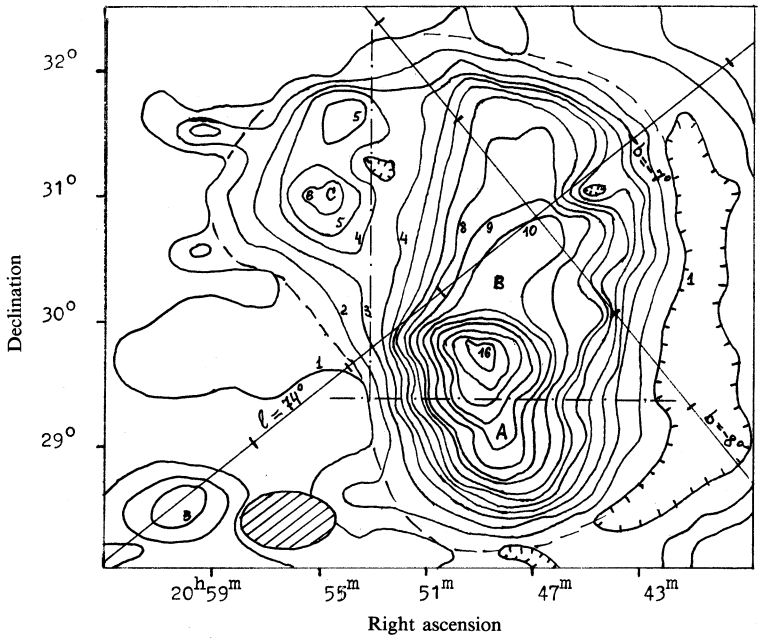

Fig. 1. Contour map of the Cygnus Loop at 102·5 MHz with CU = 2·70 Jy per beam and beam area 48′×26′. The dot–dash line is the boundary of the regions A, B and C.

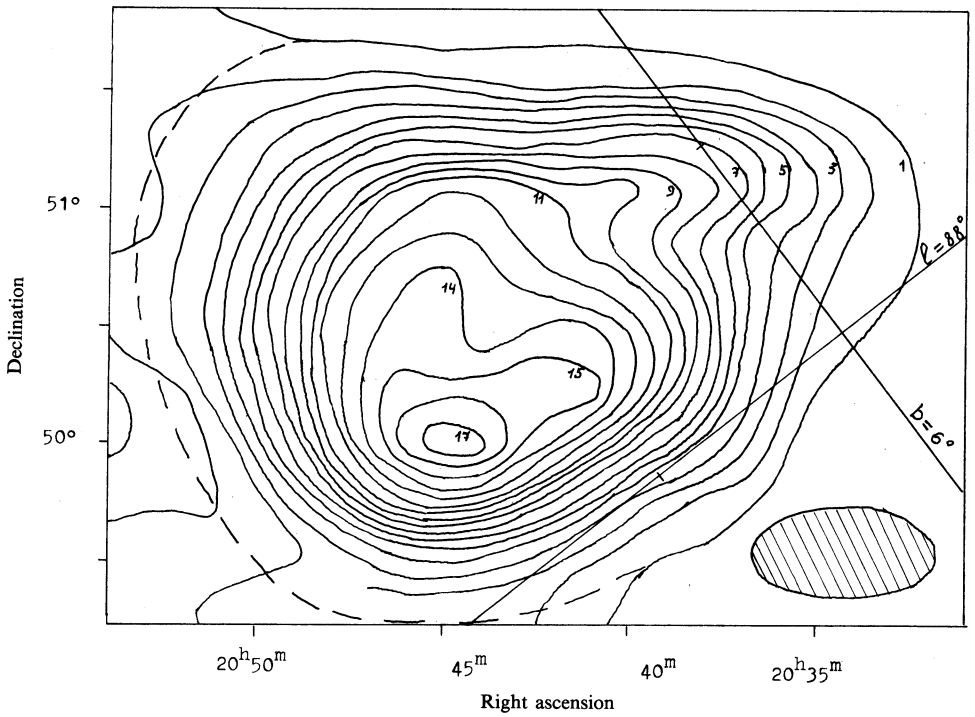

Fig. 2. Contour map of HB21 at 102·5 MHz with CU = 3·53 Jy per beam and beam area 48′×24′.

and is operated in the meridian plane at various declinations. The BSA is a multibeam instrument (16 beams in declination); adjacent beams are spaced by half a beamwidth. At 102·5 MHz the half-power beamwidths (HPBW) are 48′ and 24′ sec(55°−δ) arc in right ascension and declination respectively. Neighbouring beams overlap at a power level of 0·81. The BSA sensitivity is about 1·0 Jy in a single beam, determined chiefly by the effect of the confusion. Strip-scans obtained from each SNR passing through the 16-beam pattern were used for mapping. Maps were calibrated by discrete radio sources using the Baars scale. The full flux density for extended SNRs was obtained by integrating maps at 102·5 MHz.

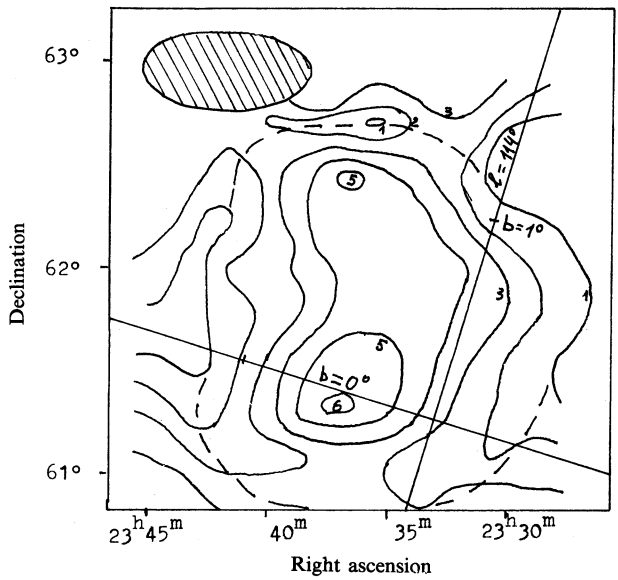

Fig. 3. Contour map of G114·3+0·3 at 102·5 MHz with CU = 1·24 Jy per beam and beam area 48′×24′.

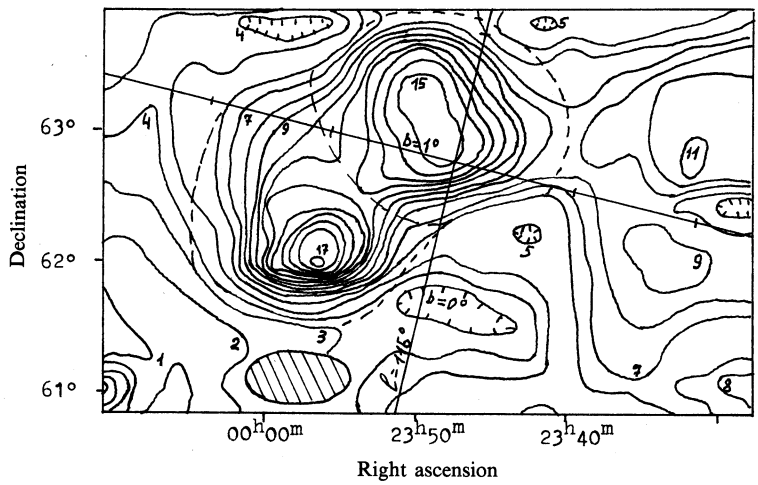

Fig. 4. Contour map of CTB1 and G116·5+1·1 at 102·5 MHz with CU = 1·65 Jy per beam and beam area 48′×24′.

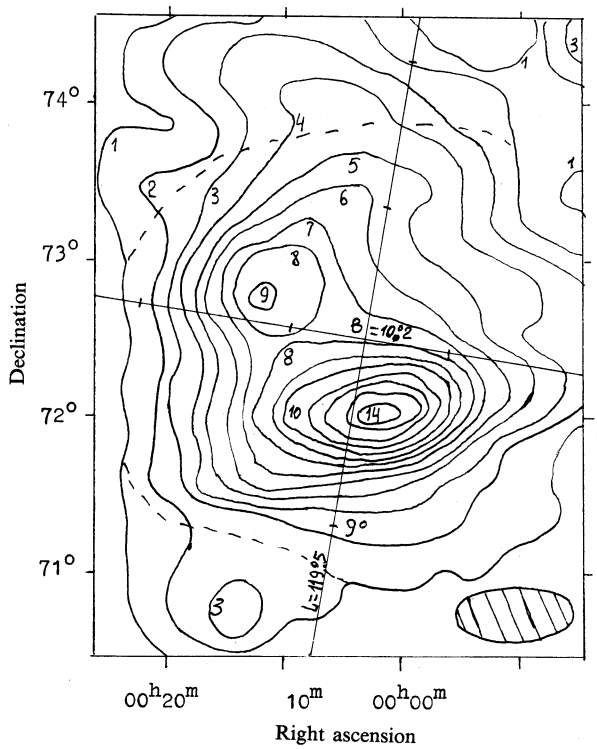

Fig. 5. Contour map of CTA1 at 102·5 MHz with CU = 1·65 Jy per beam and beam area 48′×25′.

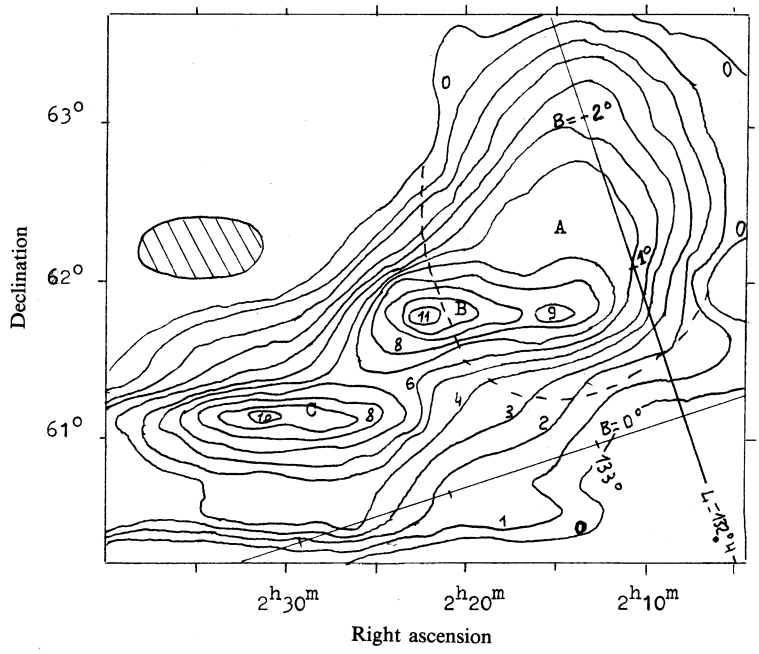

Fig. 6. Contour map of HB3 (A), 1C 1795 (B) and 1C 1805 (C) at 102·5 MHz with CU = 2·62 Jy per beam and beam area 48′×25′.

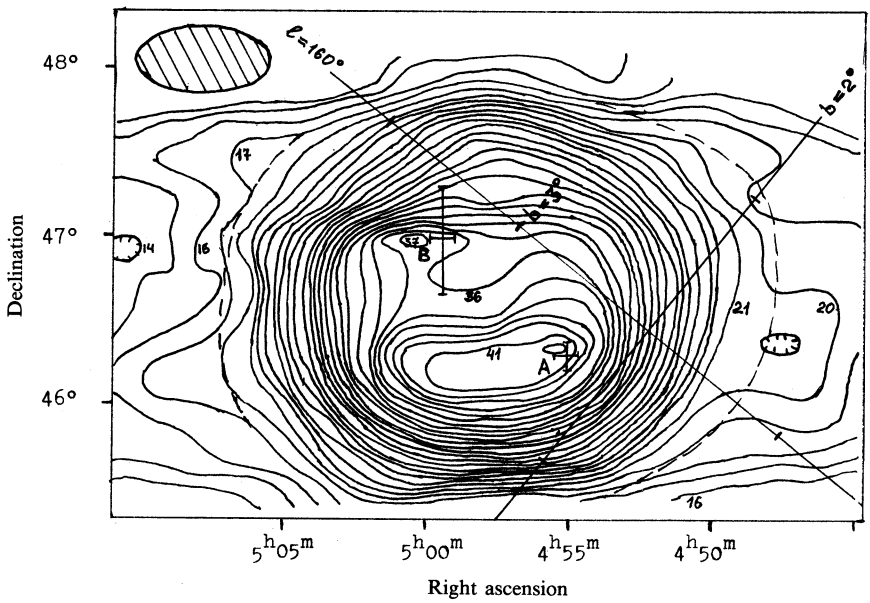

Fig. 7. Contour map of HB9 at 102·5 MHz with CU = 1·60 Jy per beam and beam area 48′×24′.

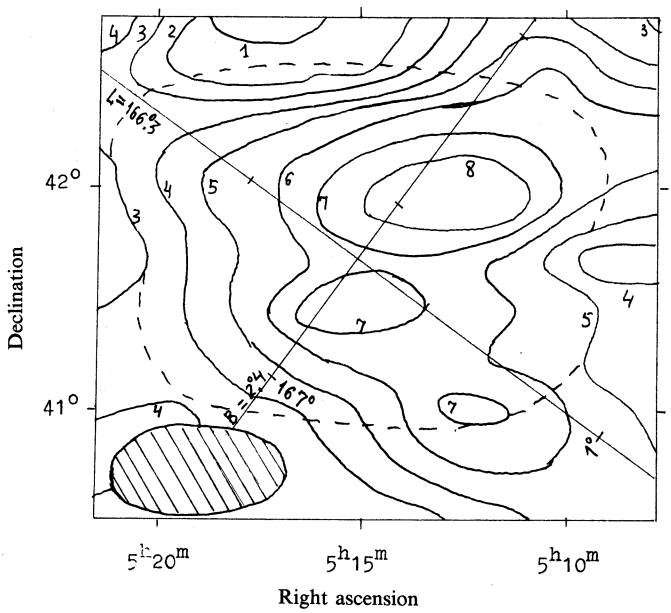

Fig. 8. Contour map of OA184 at 102·5 MHz with CU = 1·60 Jy per beam and beam area 48′×24′.

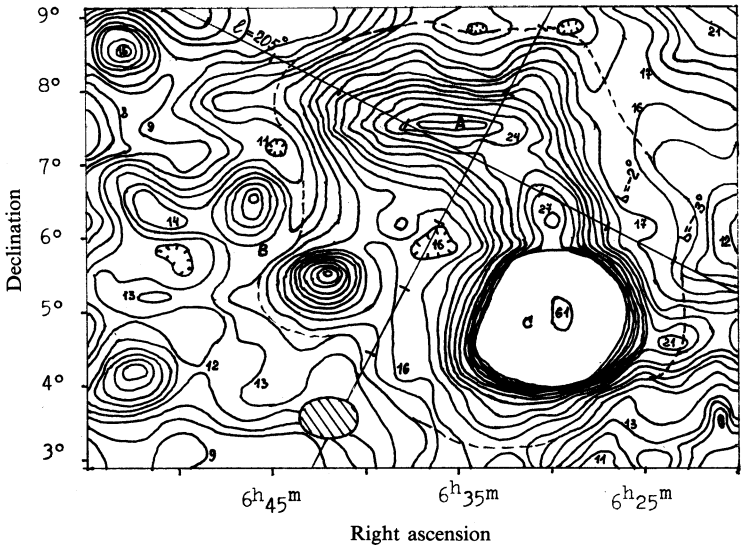

Fig. 9. Contour map of the Monoceros Loop (A) and G207·1+2·2 (B) at 102·5 MHz with CU = 1·35 Jy per beam and beam area 48′×36′.

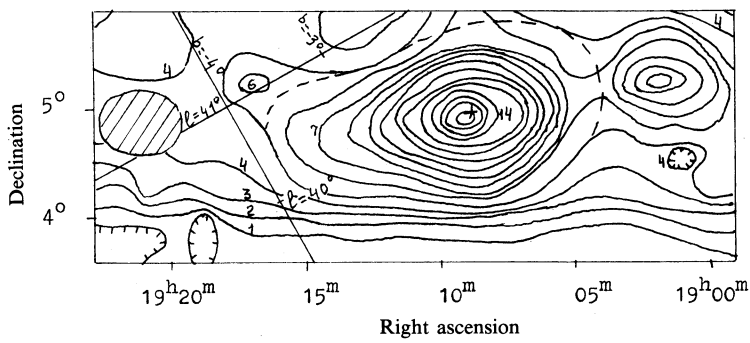

Fig. 10. Contour map of W50 at 102·5 MHz with CU = 5·75 Jy per beam and beam area 48′×37′.

3. Results

At 102·5 MHz, maps of 12 SNRs were obtained. They are shown in Figs 1–10; all coordinates are given for 1950·0. The source boundaries, within which the flux density was determined, are shown by the dashed curves. When determining the flux density of the SNRs the correction for the influence of discrete sources was made using high frequency data. The influence of discrete sources was taken into account when their flux density at 102·5 MHz was more than 1 Jy.

G74·0−8·6 (Cygnus Loop) (Fig. 1). This SNR has an angular size of 150′ and an inhomogeneous structure. This points to the fact that the SNR is highly evolved. The expanding shell has broken into several fragments, as a result of interacting with the inhomogeneous medium, and so a fragmented shell structure is obtained. The radio emission from the northern part correlates well with the optical emission. The eastern part of the SNR coinciding with the optical emission is characterised by a flat

spectrum at low frequencies (Kundu and Velusamy 1967; Udal'tsov *et al.* 1978). The bright southern part of the source is observed in the direction of very weak optical filaments. There is no X-ray emission in this direction.

G89·0+4·7 (HB21) (Fig. 2). This source has a size of about 2° and a thick shell of almost circular shape. The maximum of radio brightness is shifted towards the galactic plane. There is a discrete source 3C418 in the north-western part of this remnant.

G114·3+0·3 (Fig. 3). This is an extended SNR with a poorly defined boundary, and has the smallest surface brightness among remnants. It is suggested that this SNR is highly evolved. There is a shell structure with brightening towards the galactic plane.

G116·5+1·1 (Fig. 4). This SNR has a size of about 1° and a shell structure.

G117·3+0·1 (CTB1) (Fig. 4). Observations of this SNR at several frequencies in the centimetre band gave two values for the spectral index: 0·58 (Willis 1973) and 0·75 (Reich and Braunsfurth 1981). Most flux density observations and our 102·5 MHz data are shown in Fig. 11*a*. A spectral index of $\alpha^{2700}_{102\cdot5} = 0\cdot74$ is obtained. Our observations of CTB1 have poor resolution; however, we can see a shift of the surface brightness maximum to the galactic plane. Our contour map shows a broken shell structure.

G119·5+10·2 (CTA1) (Fig. 5). Our map at 102·5 MHz is similar to contour maps at other frequencies and shows the broken shell structure. A radio emission maximum is shifted to the galactic plane. Observations at other frequencies gave two values

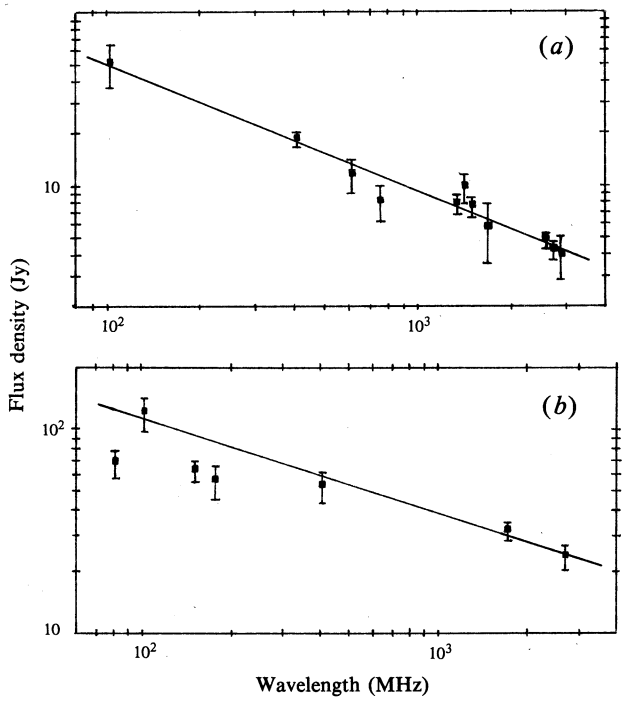

Fig. 11. Radio spectra of (*a*) CTB1 and (*b*) CTA1.

for the spectral index: 0·30 and 0·47 (Sieber *et al.* 1981). Most of the flux density observations and the 102·5 MHz value are shown in Fig. 11*b*. We have confirmed a value for the spectral index of 0·47. However, we did not include three low points (Fig. 11*b*) obtained by the method of aperture synthesis; apparently discrepancies in the spectral index are accounted for by low values of flux densities obtained by the aperture synthesis method.

G132·4+2·2 (HB3) (Fig. 6). HB3 is marked by an A in Fig. 6. Two thermal sources W3 and W4 (components B and C respectively) are observed in the vicinity of HB3. Our map shows that HB3 has a thick shell with a sharp edge to the south. This may indicate a high density of the surrounding interstellar gas in the vicinity of HB3. However, according to our data we cannot suggest an interaction of the HB3 shell with the thermal source W3.

G160·5+2·8 (HB9) (Fig. 7). This SNR has a thick circular shell with size about 2°. At 102·5 MHz there is a definite increase in brightness in the western part of the central region. This maximum is identified with the location of source 4C46·09 (A in Fig. 7). The pulsar 0458+46 (B) and a compact scintillating source 0503+46 (Pynzar' and Udal'tsov 1983*a*) are also observed in the direction of HB9. To all appearances the pulsar 0458+46 is not connected with the SNR (Pynzar' and Udal'tsov 1983*a*).

G166·2+2·5 (OA184) (Fig. 8). In the optical band OA184 is identified with a shell structure diffuse nebula of size 75′. In the radio band an inhomogeneous fragmented shell structure is observed. The 102·5 MHz integral flux density, after subtraction of the discrete source 4C42·15, is 37 Jy. The spectral index of OA184 in the band 102·5–2700 MHz is 0·53.

G205·5+0·2 (Monoceros Nebula) (Fig. 9, A). This SNR is in the shape of a loop, extending from the north of the Rosette Nebula (C) and turning to the east. An increased 102·5 MHz surface brightness is observed in the northern and western parts of the SNR. The bright Rosette Nebula restricts observations of the SNR. The source is weak and extended with an angular size about 4°. The total flux density at 102·5 MHz is 400 Jy. On the whole, the structure can be classified as fragmented shell.

G207·1+2·2 (Fig. 9). This SNR (Fig. 9 component B) is observed in a direction near to the Monoceros Loop. In the metre band the source has been observed for the first time. At 102·5 MHz the flux density is 19 Jy, the angular size is about 45′ and the spectral index is 0·50. The source is interpreted as an old and distant SNR (Graham *et al.* 1982).

G39·7–2·0 (W50) (Fig. 10). The size at the zero intensity level is 144′×62′ (in right ascension and declination respectively). This size is similar to data at high frequencies (Downes *et al.* 1981). It has a non-shell structure, similar to plerions. There is a peculiar object SS433 in the SNR centre. A compact scintillating source (marked with a cross in Fig. 10) with an angular size less than 1″ arc and a flux density for the scintillating component of 1·3±0·3 Jy for January 1983 is observed at 102·5 MHz in the centre of the SNR. This scintillating source has been identified with SS433 (Pynzar' and Udal'tsov 1983*b*). The position angle of the main axis of W50 coincides with the direction of the X-ray jet of SS433. This fact and the distribution of brightness in W50, similar to a plerion, point to a possible genetic connection of W50 with SS433. According to Watson *et al.* (1983), the distance to

SS433 is 5·1 kpc. An estimation of the distance to W50 carried out according to the Σ–$D(z)$ relation gives 2 kpc, a result which could be incorrect because of the peculiarity of W50. This peculiarity is also seen from Fig. 12. The point marked 1 corresponding to W50 strongly differs from the general group of SNRs with known diameters and adds support to the genetic connection of W50 with SS433.

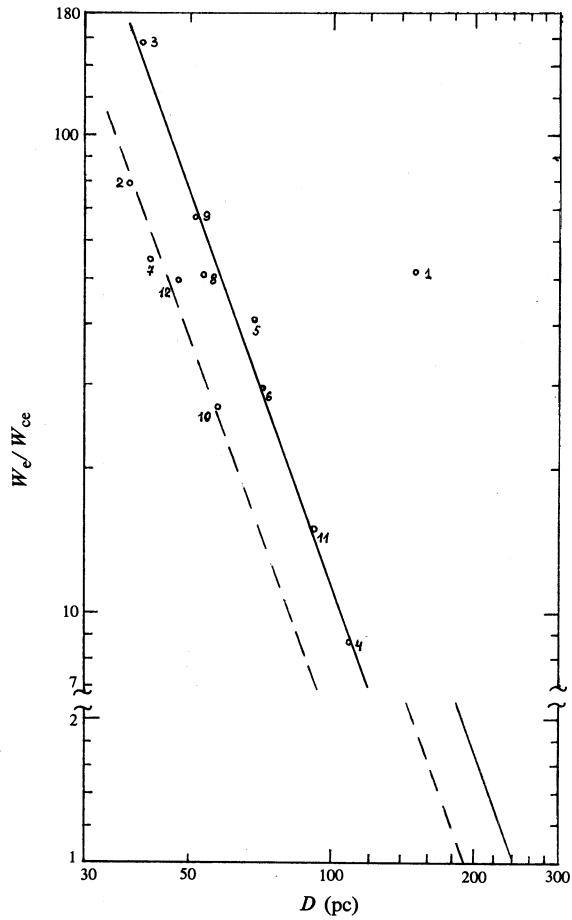

Fig. 12. The relationship W_e/W_{ce} with D, where the numbers in the figure correspond to the rows in Table 1. The straight lines have a slope of $q = -2{\cdot}85$, which corresponds to the slope of the relationship $\Sigma \sim D^{-\beta}$ [$q = -3+(17-4\beta)/7$]. The solid line corresponds to SNRs with $|z| = 49$ pc and the dashed line $|z| = 141$ pc.

The calculated and measured data of the SNRs described above are given in Table 1. The columns are as follows:

2—the effective angular size ϕ (min. arc.).

3—the integral flux density in Jy obtained by integrating contour maps within the region marked by the dashed curves in Figs 1–10. Confusing discrete sources were eliminated.

4—the surface brightness at 102·5 MHz as determined following Milne (1979).

5—the spectral index determined from the spectrum plotted using the flux density data from other authors and column 3.

Table 1. SNR data at 102·5 MHz and calculated parameters

SNR	ϕ (min. arc)	$S_{102.5}$ (Jy)	Σ (10^5 Jy sr^{-1})	α	d (kpc)	D (pc)	$\Delta R/R$	$\lvert z\rvert$ (pc)	H (10^{-5} G)	W_e (10^{47} erg)	W_{ce} (10^{46} erg)	W_e/W_{ce}	t (10^5 yr)	V_{shell} (km s^{-1})
(1)	(2)	(3)	(4)	(5)	(6)	(7)	(8)	(9)	(10)	(11)	(12)	(13)	(14)	(15)
G39·7−2·0 (W50)	100	220	3·3	0·45	5·1	148	0·25*	178	1·4.	173	33·3	51·9	—	—
G74·0−8·6 (Cyg. Loop)	150	550	3·7	0·45	0·8	37	0·16	128	2·4	5·45	0·68	80·1	0·6	94
G89·0+4·7 (HB21)	120	530	5·5	0·37	1·1	39	0·62	91	2·0	14·0	0·89	157	0·7	88
G114·3+0·3	83	13	0·28	0·32	4·4	108	0·25*	23	0·9	24·8	28·5	8·7	18·3	9
G116·5+1·1	65	77	2·7	0·85	3·6	68	0·25*	68	1·6	21·6	5·27	41·0	4·0	26
G117·3+0·1 (CTB1)	39	51	5·0	0·74	6·2	71	0·12	11	2·3	24·2	8·23	29·4	4·7	23
G119·5−10·2 (CTA1)	134	120	1·0	0·47	1·0	41	0·25	182	1·4	3·74	0·68	55·0	0·8	78
G132·4+1·2 (HB3)	84	165	3·5	0·65	2·1	53	0·25	83	1·8	12·5	2·44	51·2	1·8	44
G160·5+2·8 (HB9)	135	410	3·4	0·43	1·3	51	0·40	64	1·7	16·2	2·4	67·5	1·7	47
G166·2+2·5 (OA184)	73	37	1·0	0·53	2·6	57	0·16	117	1·4	6·73	2·51	26·8	2·3	37
G205·5+0·2 (Mon. Loop)	236	400	1·1	0·46	1·3	91	0·25	5	1·2	27·8	18·5	15·0	10·7	13
G207·1+2·2	45	19	1·4	0·50	3·5	47	0·25*	138	1·5	6·24	1·25	49·9	1·2	57

6—the distance from the Sun in kpc.

7—the linear diameter in pc.

8—the relative thickness of the shell of radius R according to the observations of Willis (1973); for the values marked with an asterisk we suggest that $\Delta R/R = 0{\cdot}25$.

9—the distance modulus from the galactic plane in pc; the parameters in columns 6, 7 and 9, except for W50, are calculated according to the Σ–$D(z)$ relation by Milne (1979).

10—the magnetic field H within the SNR shell estimated from the equipartition condition of energies in the magnetic field and relativistic particles.

11—the energy of relativistic electrons in the SNR shell responsible for the observed radio emission; W_e is estimated from our data and from the formula (Ginzburg 1975)

$$W_e = 0{\cdot}19\kappa_H^{-3/7}\,\kappa_e^{-1}\{\kappa_e\,A(\alpha,\nu_1,\nu_2)\,S_{102{\cdot}5}\,d^2\}^{4/7}D_{\text{eff}}, \qquad (1)$$

where $\kappa_e = 100$ and $\kappa_H = 1$ are the constants of proportionality in the equipartition condition of energies of particles and H fields, $S_{102{\cdot}5}$ is the flux density at 102·5 MHz, d is the distance to a SNR, $\nu_1 = 10$ MHz, $\nu_2 = 10^4$ MHz, D_{eff} is the effective diameter of the radio emission sphere with volume equal to the shell volume with thickness ΔR, and is determined using the data in columns 7 and 8 of Table 1, and $A(\alpha,\nu_1,\nu_2)$ is a coefficient taken from Ginzburg (1975).

12—the energy of interstellar medium relativistic electrons in the SNR volume at height z above the galactic plane. The energy is estimated from $W_{ce} = \kappa_e^{-1}\,W_{ch} = \kappa_e^{-1}\,D^3H_c(z)/48$, where $H_c(z) = H_0\exp(-|z|/z_{ch})$ is the interstellar H field. The value $z_{ch} = 400$ pc is determined from the condition $H_c \sim \rho^{0{\cdot}45}$ (Brown and Chang 1983), where $\rho = \rho_0\exp(-|z|/z_\rho)$ and $z_\rho = 180$ pc is the scale size of the change of the galactic intercloud gas density ρ with z (Falgarone and Lequeux 1973). On the average, ρ determines the dynamics of SNRs (Lozinskaya 1980). The interstellar electron energy density at $z = 0$ was taken as 10^{-14} erg cm^{-3} (Ginzburg 1975).

13—the ratio of W_e to W_{ce}.

14—the SNR age in 10^5 yr.

15—the velocity of the shell expansion in km s^{-1}. The values in columns 14 and 15 were obtained from the model by Chevalier (1974).

4. Discussion

Results of our observations and calculated data from Table 1 show that all (except W50) investigated SNRs are shell type. These SNRs have ages $>10^4$ yr, diameters $\gtrsim 40$ pc, expansion velocities <100 km s^{-1} and surface brightnesses $<6\times10^{-21}$ W m^{-2} Hz^{-1} sr^{-1}. All these facts suggest that the SNRs are at a late stage of evolution. Values of W_e/W_{ce} for these objects are in the range 8–150. If for late stage evolution of SNRs the equipartition condition $\kappa_e\,W_e = W_H$ is correct (Ginzburg 1975), then for all SNRs in Table 1 the predominant source of radiation is relativistic electrons which are genetically connected with the SNR. The contribution to the observed radiation of old SNRs from swept up cosmic ray electrons is small (column 13).

Relativistic electrons which are genetically connected with SNRs might be produced by a supernova, either by continuous emission from the relic star of the supernova, such as the Crab pulsar, or by acceleration in the SNR shell.

For old SNRs the process of acceleration appears to be the most likely source for electrons radiating at radio frequencies. The other interpretation of particles from the SN outburst does not explain the situation because the lifetime is small for these electrons. Emission from a relic star does not explain the situation either, as searches for star remnants (pulsars, X-ray and scintillating sources) within old SNRs (Pynzar' and Udal'tsov 1981, 1983*b*) have not been positive (excluding W50).

In Fig. 12 the dependence of W_e/W_{ce} on diameter is shown. The two straight lines correspond to SNRs with an average height from the galactic plane of $z = 49$ pc and 141 pc. From Fig. 12 we can estimate the sizes of SNRs when the energy of relativistic electrons swept up from the interstellar medium by the SNR expansion is equal to the radiating particle energy. These sizes are 200–250 pc (Fig. 12). Excluding Loops I–IV, radio SNRs with such sizes in the Galaxy have not been observed. This implies that in the Galaxy there must be many old SNRs with sizes about 100–200 pc, which we cannot observe as radio SNRs. The existence of Heiles's HI shells and supershells in the Galaxy supports this conclusion.

References

Brown, R. L., and Chang, C.-A. (1983). *Astrophys. J.* **264**, 134.
Chevalier, R. A. (1974). *Astrophys. J.* **188**, 501.
Downes, A. J., Pauls, T., and Salter, C. J. (1981). *Astron. Astrophys.* **103**, 277.
Falgarone, E., and Lequeux, J. (1973). *Astron. Astrophys.* **25**, 253.
Ginzburg, V. L. (1975). 'Theoretical Physics and Astrophysics', pp. 90–95 (Nauka: Moscow).
Graham, D. A., Haslam, C. G. T., Salter, C. J., and Wilson, W. E. (1982). *Astron. Astrophys.* **109**, 145.
Gull, S. F. (1973). *Mon. Not. R. Astron. Soc.* **161**, 47.
Kundu, M. R., and Velusamy, T. (1967). *Ann. Astron.* **30**, 723.
Lozinskaya, T. A. (1980). *Astron. Astrophys.* **84**, 26.
Milne, D. K. (1979). *Aust. J. Phys.* **32**, 83.
Pynzar', A. V., and Udal'tsov, V. A. (1981). *Astron. Zh.* **58**, 1177.
Pynzar', A. V., and Udal'tsov, V. A. (1983*a*). *Astron. Zh.* **60**, 493.
Pynzar', A. V., and Udal'tsov, V. A. (1983*b*). Fifteenth Conf. on USSR Galactic and Extragalactic Radioastronomy, Abstracts, Moscow, p. 131.
Reich, W., and Braunsfurth, E. (1981). *Astron. Astrophys.* **99**, 17.
Shklovskii, I. S. (1960). *Sov. Astron.* **37**, 256.
Sieber, W., Salter, C. J., and Mayer, C. J. (1981). *Astron. Astrophys.* **103**, 393.
Udal'tsov, V. A., Pynzar', A. V., and Glushak, A. P. (1978). *Usp. Fiz. Nauk* **124**, 725.
Van der Laan, H. (1962). *Mon. Not. R. Astron. Soc.* **124**, 125.
Vitkevich, V. V., Glushaev, A. A., Ilyasov, Yu. P., Kutuzov, S. M., Kuzmin, A. D., Alekseev, I. A., Bunin, V. D., Novozhenov, G. F., Pavlov, G. A., Solomin, H. S., and Tyaptin, M. M. (1976). *Radiofizika* **19**, 1594.
Watson, M. C., Willinale, R., Grinlay, J. E., and Seward, F. D. (1983). *Astrophys. J.* **273**, 688.
Weiler, K. W., and Panagia, N. (1978). *Astron. Astrophys.* **70**, 419.
Willis, A. G. (1973). *Astron. Astrophys.* **26**, 237.

Manuscript received 19 March, accepted 20 October 1987